

# Spatial-Domain Technique to Overcome Grating Lobes in Sparse Monostatic mm-Wave Imaging Systems

B. Mamandipoor\*, M. Fallahpour†, G. Malysa‡, K. Noujeim‡, U. Madhow\* and A. Arbabian†

\* ECE Department, University of California, Santa Barbara, CA, USA

† EE Department, Stanford University, Stanford, CA, USA

‡ Microwave Measurements Division, Anritsu Co., Morgan Hills, CA, USA

Emails: {bmamandi, madhow}@ece.ucsb.edu, Karam.Noujeim@anritsu.com,

{mfall, gmalysa, arbabian}@stanford.edu

**Abstract**—In this work, a spatial-domain technique is introduced to mitigate grating lobes in sparse monostatic arrays targeting applications such as low-cost real-time mm-wave imaging systems. Standard algorithms, such as synthetic aperture radar (SAR) techniques, are susceptible to grating lobes and result in images with significantly degraded quality. In order to suppress artifacts due to the grating lobes, a new spatial aggregation technique is introduced, which replaces point-scatterer based basis function by a new set of spatially extended basis functions. The efficacy of the proposed method is demonstrated using experimental data. Our hardware testbed is a 60 GHz continuous-wave radar transceiver, equipped with a movable mechanical platform to emulate a 2-dimensional array of sensors.

## I. INTRODUCTION

There is growing interest in the development of high resolution real-time mm-wave imaging systems with commercial, medical, and security screening applications [1], [2], [3], [4]. In order to achieve real-time operation, data collection via mechanical raster scan must be replaced by an actual array of antenna elements. However, due to complexity, weight and cost considerations, the number of elements in such arrays should be reduced to the extent possible. This results in sparse arrays [1], [5] producing spatially undersampled signals, resulting in imaging characteristics that are quite different from those of a dense array in the same physical aperture. In particular, when the data collected by a sparse array is processed using conventional SAR-like algorithms, the imaging performance deteriorates significantly because of grating lobes. A multistatic architecture, where the elements are synchronized across the array, provides a dense *effective* aperture that removes grating lobes [2]. However, synchronizing spatially dispersed array elements at mm-wave frequencies is challenging and leads to a significant increase in the cost and complexity of the design. In this paper, therefore, we restrict attention to a monostatic architecture, and show that it is possible to alleviate grating lobes by rethinking the target models, and the associated imaging algorithms.

Existing approaches to grating lobe suppression include the use of shaped waveforms, aperture diversity, pulse diversity, frequency diversity (wideband), and digital spotlighting [6], [7], [8]. However, to our knowledge, there is little prior work on improving the scene/target model to handle spatial undersampling. In fact, almost all imaging techniques

have been developed based on a point scatterer target model [9]. This includes popular variants of SAR-based imaging algorithms in both the spatial-temporal domain (e.g., time-domain correlation or exact matched-filtering) and the spatial-frequency domain (e.g., wavenumber or  $\omega$ - $k$  algorithm)[6]. In this paper, we show that grating lobes can be suppressed by modifying the point scatterer target model, replacing it with “patches” formed by spatial aggregation of points. We illustrate our results for a sparse monostatic array for short-range (sub-meter) continuous-wave imaging. We modify the matched-filtering SAR technique for the new patch-based basis functions, and demonstrate the gains in imaging performance through experimental data collected using a 60 GHz prototype.

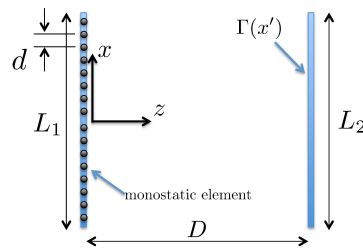


Fig. 1. Geometry of 1-dimensional monostatic imaging configuration.

## II. PROBLEM STATEMENT

A typical imaging configuration with 1-D array for data collection is depicted in Fig. 1. Let  $L_1$ ,  $L_2$ , and  $D$  denote the size of the aperture, the size of the scene, and the distance between the aperture and the scene, respectively. We consider the nominal values  $L_1 = L_2 = 15\text{cm}$  and  $D = 30\text{cm}$  in our simulations. The inter-element spacing of a uniform linear array comprised of  $N$  elements is given by  $d = L_1/(N - 1)$ . Assume  $\Psi$  to be a set that contains the locations of all the point scatterers in the scene, and  $\Gamma(x')$  denote the complex reflection coefficient corresponding to the point scatterer at location  $x'$  (primed coordinate indicates location of the target). The scene response collected at the aperture is an  $N$ -dimensional vector denoted by  $r \in \mathbb{C}^N$ , for which the  $n^{\text{th}}$  entry corresponds to the monostatic transceiver located at  $x_n$ , and is given by,

$$r[n] = \int_{x' \in \Psi} \Gamma(x') e^{-j2kR(x', x_n)} dx', \quad (1)$$

where  $k = 2\pi/\lambda$  is the wavenumber, and  $R(x', x_n) = \sqrt{D^2 + (x' - x_n)^2}$  is the path length from the transceiver location to the point scatterer at location  $x'$ . Using a first order Taylor approximation, the path length is calculated as,  $R(x', x_n) \approx D + \frac{(x' - x_n)^2}{2D}$ . Therefore,

$$r[n] \approx e^{-j2kD} \int_{x' \in \Psi} \Gamma(x') e^{-j\frac{k}{D}(x' - x_n)^2} dx'. \quad (2)$$

The grating lobes appear when two distinct point scatterers in the scene generate highly correlated responses. In SAR imaging, a (virtual) testing point is moved over the entire imaging domain and the response at the aperture for each hypothesized position is calculated. An image of the scene is constructed by correlating this dictionary of template responses with the measured response. Now, consider a fixed point scatterer (i.e., target) located at  $x'_1$  and a testing point  $x'_2$ , with the responses denoted by  $r_1$  and  $r_2$ , respectively. The correlation between the two responses is calculated as,

$$\begin{aligned} r_1^H r_2 &= \sum_{n=1}^N \Gamma_1^* \Gamma_2 e^{j\frac{k}{D}(x'_1 - x_n)^2} e^{-j\frac{k}{D}(x'_2 - x_n)^2} \\ &= \Gamma_1^* \Gamma_2 e^{j\frac{k}{D}(x'_1{}^2 - x'_2{}^2)} \sum_{n=1}^N e^{j\frac{2k}{D}(x'_2 - x'_1)x_n} \\ &= c_1 \frac{\sin(N\rho/2)}{\sin(\rho/2)} = c_1 \text{Dir}(\rho), \end{aligned} \quad (3)$$

where  $c_1$  is a complex coefficient with  $|c_1| = |\Gamma_1||\Gamma_2|$ , and  $\text{Dir}(\rho) = \frac{\sin(N\rho/2)}{\sin(\rho/2)}$  is the well-known Dirichlet kernel with  $\rho \triangleq \frac{2k}{D}(x'_2 - x'_1)d$ . Note that  $\rho \in [0, 2kdL_2/D]$ , this means that it takes values in an interval that depends on the signal wavelength and the geometry of the imaging problem. On the other hand, the Dirichlet kernel is a periodic function with period  $2\pi$ . Therefore, the condition for avoiding grating lobes translates to constraining the visible range of  $\rho$  to be less than  $2\pi$  (i.e.,  $\frac{2kdL_2}{D} \leq 2\pi$ ), which yields  $\frac{2L_1L_2}{D\lambda} + 1 \leq N$ . For our nominal parameter values, this leads to  $N \geq 31$ . We should mention that  $\frac{2L_1L_2}{D\lambda} + 1$  is the total number of spatial *degrees of freedom* imposed by the geometry of the imaging problem and wavelength. Figure 2 shows the magnitude of the normalized correlations for point scatterer being fixed at  $x'_1 = 4\text{cm}$ , and testing point at  $x'_2 \in [-7.5, 7.5]\text{cm}$ , for  $N \in \{15, 31\}$ . It can be seen that setting  $N = 15$  leads to a grating lobe artifact at  $x'_{\text{gl}} \approx -3.5\text{cm}$ . The separation between the true point location and the grating lobe is calculated by setting  $\rho = 2m\pi$ , for  $m \in \mathbb{Z}$ . It is easy to see that the first grating lobe is at distance  $\Delta x = |x'_{\text{gl}} - x'_1| \approx \frac{\lambda D}{2d}$  from the true point location (e.g.  $\Delta x \approx 7.5\text{cm}$  for  $N = 15$ ).

### III. GRATING LOBE SUPPRESSION VIA SPATIAL AGGREGATION

The main contribution of this paper is in introducing a new set of basis functions to suppress grating lobe artifacts in a sparse monostatic array. The idea is to replace the point scatterer as the basis function for explaining the scene, with a collection of point scatterers, adjacent to one another and

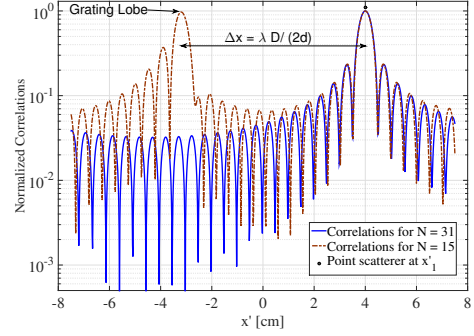


Fig. 2. Grating lobe artifact for sparse monostatic array.

having constant (appropriately weighted) reflection coefficient. This is a natural model for explaining extended objects with bounded variation in the reflectivity function  $\Gamma(x')$  across space; that is, for scenes where the reflectivity is a *spatially lowpass* function. Let us consider two collection of point scatterers  $\Psi_1$  and  $\Psi_2$ , with their corresponding responses denoted by  $r_{\Psi_1}$  and  $r_{\Psi_2}$ , respectively. The correlation between the two responses is calculated as follows,

$$\begin{aligned} r_{\Psi_1}^H r_{\Psi_2} &= \sum_{n=1}^N \int_{x'_1 \in \Psi_1} \Gamma^*(x'_1) e^{j2kR(x'_1, x_n)} dx'_1 \int_{x'_2 \in \Psi_2} \Gamma(x'_2) e^{-j2kR(x'_2, x_n)} dx'_2 \\ &\approx \iint_{\substack{x'_1 \in \Psi_1 \\ x'_2 \in \Psi_2}} \Gamma^*(x'_1) \Gamma(x'_2) e^{j\frac{k}{D}(x'_1{}^2 - x'_2{}^2)} \sum_{n=1}^N e^{j\frac{2k}{D}(x'_2 - x'_1)x_n} dx'_2 dx'_1 \\ &= c_2 \iint_{\substack{x'_1 \in \Psi_1 \\ x'_2 \in \Psi_2}} \Gamma^*(x'_1) \Gamma(x'_2) H(x'_1, x'_2) \text{Dir}(\rho) dx'_2 dx'_1, \end{aligned} \quad (4)$$

where  $c_2$  is a constant, and  $H(x'_1, x'_2) \triangleq e^{j\frac{k}{D}(x'_1{}^2 - x'_2{}^2)}$  is the Spatial Aggregation (SA) kernel. The magnitude of SA kernel is constant, and the phase is a non-linear function of  $x'_1$  and  $x'_2$ . Figure 3 shows the magnitude of the Dirichlet kernel, the phase of SA kernel, as well as the phase of the product  $H(x'_1, x'_2) \text{Dir}(\frac{2k}{D}(x'_2 - x'_1)d)$  for  $x'_1, x'_2 \in [-7.5, 7.5]\text{cm}$ . The key observation is that the phase of SA kernel is nearly constant across the main lobe, whereas it exhibits fast variations across the grating lobes. Therefore, spatial aggregation significantly suppresses the grating lobes due to the incoherency induced by the SA kernel.

In order to illustrate the effect of spatial aggregation, in a case study, consider a fixed extended target  $\Psi_1 = [3.5, 4.5]\text{cm}$  at distance  $D$  from the array, and the collection of basis functions defined by  $\Psi_2 = [\alpha - 0.5, \alpha + 0.5]\text{cm}$  for all  $\alpha \in [-7.5, 7.5]\text{cm}$ . In other words,  $\Psi_2$  is a moving strip (or 1D patch) of 1cm width and we generally call this new basis as *patch basis function*. Figure 4 shows the normalized correlations for the collections of 1cm patches along with that of point scatterers for  $N = 15$ . The effect of SA is three-fold;

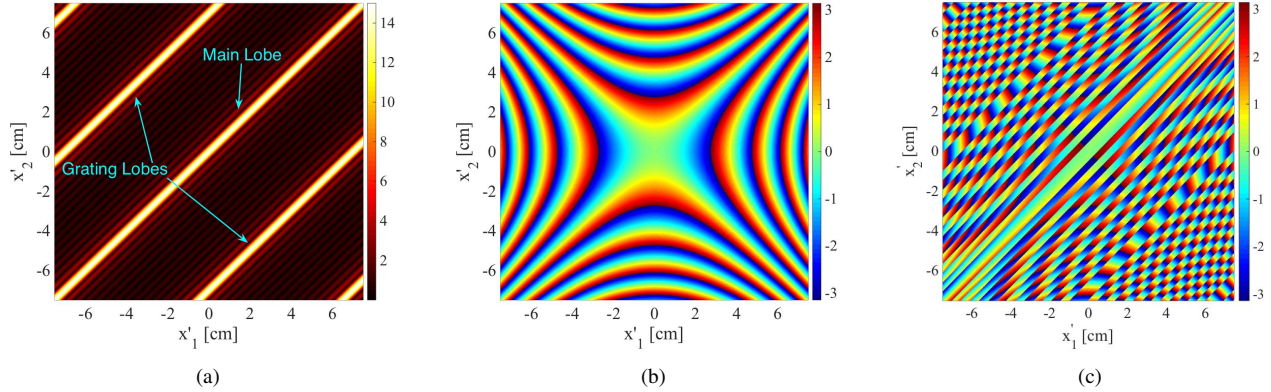


Fig. 3. (a) Magnitude of Dirichlet ( $N = 15$ ), (b) Phase of SA kernel, (c) Phase of the product of SA kernel and Dirichlet kernel  $H(x'_1, x'_2)\text{Dir}(\rho)$ .

(1) suppressing the grating lobe, (2) reducing the side lobe level (hence increasing the dynamic range of the image), and (3) widening the main lobe. It is important to note that the main lobe of patch correlations is representing an extended object, therefore, its width should be analyzed with respect to the width of the patch itself. In our specific example, we see that  $-3\text{dB}$  width of the main lobe is approximately equal to the size of the patch.

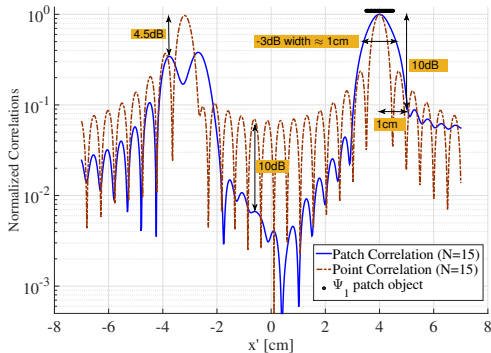


Fig. 4. Reduction of grating/side lobes by spatial aggregating.

The proposed spatial aggregation method explicitly incorporate the information about the geometry of the imaging system and the nature of the aperture in forming the image. Moreover, the prior information regarding the nature of the targets (e.g., shape/size/type) can be used for choosing the proper basis functions that are well-matched to the scene. We now focus on 2D cross-range imaging of a simple scene and demonstrate the efficacy of spatial aggregation method in reducing the grating lobes using experimental data.

#### IV. EXPERIMENTAL RESULTS

Our hardware testbed is a 60 GHz continuous-wave radar transceiver, equipped with dual high-gain horn antennas [10]. A mechanical platform was used to move the antenna on a plane parallel to the scene, hence emulating a 2-dimensional

array of sensors. The scanned area by the antenna is on the order of the form factor of a portable handheld device (covering a  $15\text{cm} \times 15\text{cm}$  area). Three uniform planner array configurations were considered: (I) super-dense array of  $75 \times 75$  elements (i.e.  $d = 0.4 \times \lambda = 0.2\text{cm}$ ), (II) dense array of  $30 \times 30$  elements (i.e.  $d = \lambda = 0.5\text{cm}$ ), (III) sparse array of  $15 \times 15$  elements (i.e.  $d = 2\lambda = 1\text{cm}$ ). At each step of the movement, the sample under test's response (which is a complex number) is measured and stored in a vector. The sample is built using copper strips mounted on cardboard and placed parallel to the array at a distance  $D = 30\text{cm}$  (Figure 5).

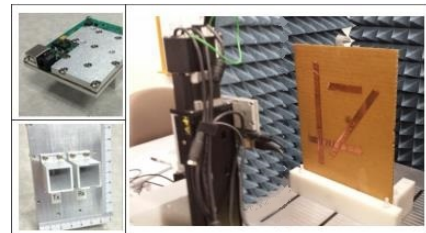


Fig. 5. Experimental data collection using 60 GHz radar system (figure is not at scale).

The first image reconstruction algorithm that we use is the standard SAR method, which works based on matched-filtering (MF) with respect to a point scatterer model for the scene [6]. The second method, is our proposed patch-based SAR, which operates based on MF with respect to a patch basis functions. For the experiments in this paper, we use  $1\text{cm} \times 1\text{cm}$  square patches as the basis functions. Future work will include criteria for choosing an appropriate patch size as a function of the geometry of the imaging problem, sparsity level of the array, and the nature of the scene. Figure 6 shows the results of point and patch-based MF for super-dense array architecture. The grating lobes do not appear for either of point or patch based reconstruction techniques. The patch MF, however, is able to reduce the side lobe levels compared to the point-based approach, hence producing a very clean image. Figures 7 and 8 correspond to the dense and sparse array architectures, respectively. We

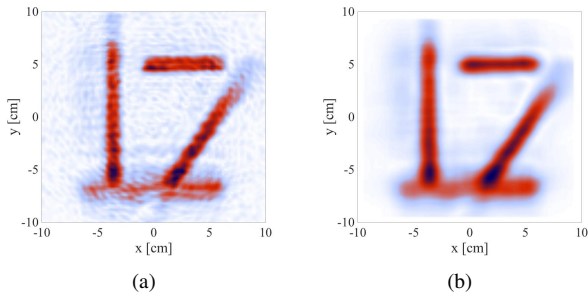


Fig. 6. Super-dense array I (a) Point MF (b) Patch MF (1cm  $\times$  1cm).

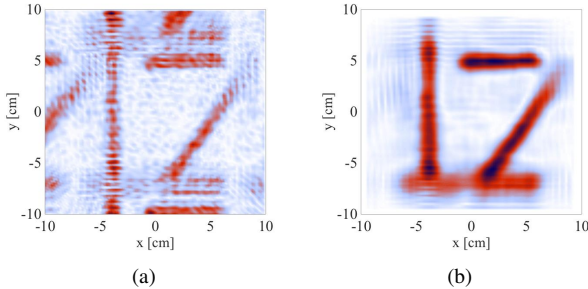


Fig. 7. Dense array II (a) Point MF (b) Patch MF (1cm  $\times$  1cm).

see that the grating lobes and side lobes exist for the point-based SAR, with their effects being significantly destructive for the sparse array. Note that the location of the grating lobes is well approximated by  $\Delta x \approx \frac{\lambda D}{2d}$ . For the patch-based SAR method, a significant improvement can be seen in the image quality, in terms of suppressing the grating lobes and increasing the dynamic range (e.g., the horizontal strip at the bottom of the scene remains visible). It should be mentioned that the idea of spatial aggregation had been developed in the spatial domain and it has differences with other ideas developed in spatial-frequency domain (e.g., filtered back-projection methods). After extending this framework to spatial-frequency domain, a comparison with those methods can be performed. Another important point is that the SA method exploits the lowpass structure of typical scenes in the spatial-frequency domain in order to mitigate the aliasing effects of array sub-sampling. Therefore, the spatial-frequency content of the scene imposes a limit on the minimum number of array elements that we need to capture the desired information from the scene. We should also mention that the SA technique provides a general framework for designing basis functions that allow for *sparse representation* of simple scenes. This parsimonious representation, with appropriately designed estimation algorithms, allows us to “super-resolve” beyond the limits of conventional radar theory. Future work will include such extensions of the SA technique.

## V. CONCLUSION

The grating lobe problem in continuous-wave monostatic imaging was investigated and its effect on conventional spatial-temporal domain SAR techniques was characterized. It was

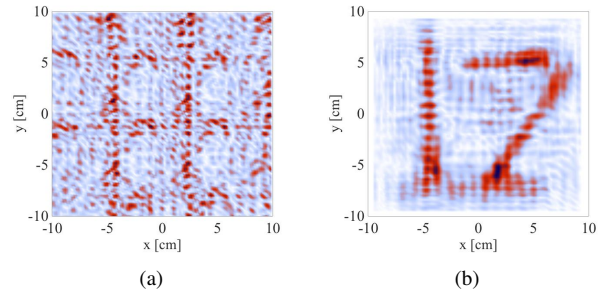


Fig. 8. Sparse array III (a) Point MF (b) Patch MF (1cm  $\times$  1cm).

shown that replacing point scatterer basis function with appropriate basis functions can help significantly suppress grating/side lobes and consequently improve the image resolution, quality, and dynamic range. For future work, we will work on characterizing the optimum shape and size of the aggregating regions (e.g., size and shape of the patches). Also, to achieve a fast imaging method for real-time applications, extension of the idea to the spatial-frequency domain will be investigated.

## VI. ACKNOWLEDGEMENT

This work was supported in part by Systems on Nanoscale Information fabriCs (SONIC), one of the six SRC STARnet Centers, sponsored by MARCO and DARPA, by Texas Instruments Inc., and by the National Science Foundation under grants CNS-1518812 and CNS-1518632.

## REFERENCES

- [1] S. S. Ahmed, A. Schiessl, L. Schmidt, “A novel fully electronic active real-time imager based on a planar multistatic sparse array,” *IEEE Transactions on Microwave Theory and Techniques*, vol.59, no.12, pp.3567-3576, Dec. 2011.
- [2] S. S. Ahmed, A. Schiessl, L. Schmidt, “Novel fully electronic active real-time millimeter-wave imaging system based on a planar multistatic sparse array,” *IEEE MTT-S International Microwave Symposium Digest*, pp.1-4, June 2011.
- [3] A. Arbabian, S. Callender, S. Kang, M. Rangwala, and A. Niknejad, “A 94 ghz mm-wave-to-baseband pulsed-radar transceiver with applications in imaging and gesture recognition,” *IEEE Journal of Solid-State Circuits*, vol. 48, pp. 1055-1071, April 2013.
- [4] M. Fallahpour, R. Zoughi, “Fast 3-D qualitative method for through-wall imaging and structural health monitoring,” *IEEE Geoscience and Remote Sensing Letters*, vol.12, no.12, pp.2463-2467, Dec. 2015.
- [5] B. Mamandipoor, G. Malysa, A. Arbabian, U. Madhow, and K. Noujeim, “60 ghz synthetic aperture radar for short-range imaging: Theory and experiments,” in *48th Asilomar Conference on Signals, Systems and Computers*, pp. 553-558, Nov 2014.
- [6] D. W. Hawkins, “Synthetic aperture imaging algorithms: with application to wide bandwidth sonar,” Ph.D. thesis, University of Canterbury, Christchurch, New Zealand, 1996.
- [7] J. Camacho, M. Parrilla, and C. Fritsch, “Phase coherence imaging,” *IEEE Trans. Ultrason. Ferroelectr. Freq. Control*, vol. 56, no. 5, pp. 958-974, 2009.
- [8] C. Martin, O. Martinez, L. Ullate, A. Octavio, and G. Godoy, “Reduction of grating lobes in saft images,” in *Ultrasonics Symposium, 2008. IUS 2008. IEEE*, pp. 721-724, 2008.
- [9] M. Fallahpour, J. T. Case, M. Ghasr, and R. Zoughi, “Piecewise and wiener filter-based SAR techniques for monostatic microwave imaging of layered structures,” *IEEE Transactions on Antennas and Propagation*, vol. 62, no. 1, pp. 1-13, Jan. 2014.
- [10] K. Noujeim, G. Malysa, A. Babveyh, and A. Arbabian, “A compact nonlinear-transmission-line-based mm-wave sfew imaging radar,” in *44th European Microwave Conference (EuMC)*, pp. 1766-1769, 2014.